Available online at www.sciencedirect.com
ScienceDirect
Journal of Luminescence 127 (2007) 371–376
JOURNAL OF LUMINESCENCE
www.elsevier.com/locate/jlumin

Photoluminescence properties of samarium-doped TiO_2 semiconductor nanocrystalline powders

Lanying Hu, Hongwei Song*, Guohui Pan, Bin Yan, Ruifei Qin, Qilin Dai, Libo Fan, Suwen Li, Xue Bai

Key Laboratory of Excited State Physics, Changchun Institute of Optics, Fine Mechanics and Physics, Chinese Academy of Sciences, and Graduate School of Chinese Academy of Sciences, 16 Eastern Nan-Hu Road, Changchun 130033, PR China

Received 24 August 2006; received in revised form 12 January 2007; accepted 18 January 2007
Available online 20 February 2007

Abstract

In this work, the luminescence properties of samarium ions-doped titanium dioxide prepared by the sol–gel process were studied. A strong orange red emission ($^4G_{5/2}$–$^6H_{7/2}$ (orange) and $^4G_{5/2}$–$^6H_{9/2}$ (red)) ascribed to the electron transitions in $4f^5$ configuration of Sm^{3+} ions was observed upon excitation into TiO_2 host. The energy transfer from TiO_2 to Sm^{3+} was verified and the relevant mechanism was discussed. In addition, the impacts of metal ion codopants upon the TiO_2:Sm^{3+} luminescence properties were studied. The results indicated that the central excitation band shifted to blue in the bismuth-codoped materials (0.5–4% in molar ratio), while it shifted to red in the zirconium-codoped materials. Such materials may find applications in white light-emission diode (LED) and tunable solid lasers.

Keywords: TiO_2:Sm; Luminescence; Sol–gel method; Metal ion codopants; Energy transfer

1. Introduction

Rare-earth (RE)-doped materials display usage in a wide variety of applications, including phosphors, X-ray imaging, scintillators, lasers, display monitors, and amplifiers for fiber-optic communications [1]. Up to date, a variety of materials have been investigated as the host lattice for RE cations, including oxides, sulfides, selenides, and metallorganic complexes. Some semiconductors including AlN [2,3], GaN [4], ZnO [5], ZrO_2 [6], and TiO_2 [7,8] might be attractive hosts for RE ions because of their relatively wide band gaps and high refractive indices.

Considering the relatively wide band gaps (3.0 eV for rutile and 3.2 eV for anatase) [9], high refractive indices ($n = 2.52$ for anatase phase and $n = 2.76$ for rutile phase) and lower phonon energy ($<700\,cm^{-1}$) [10], TiO_2 is a good candidate to be used as the host material of RE in order to excite RE ions efficiently and to yield intense luminescence. Various RE ions (Sm [11–13], Er [14], Eu [15–19], and Tb [20]) have previously been incorporated into sol–gel-prepared TiO_2 and their optical properties have been studied. Kiisk et al. [11–13] prepared a set of Sm-doped TiO_2 thin films by sol–gel method. Relaxation of electronic excitations and the energy transfer process to Sm^{3+} ions were discussed. Metal ions could be conveniently substituted into the TiO_2 lattice if their ionic radii are comparable to that of the Ti^{4+} cations. Inserting dopants into TiO_2 lattice should affect the photo-absorption behavior of TiO_2. Inspired by the sensitization of photoanode through the doping of metal ion in TiO_2 photocatalyst [21], we dedicated to synthesize a kind of material whose excitation wavelength can be tuned. Such materials might meet the need of white light-emission diode (LED) and tunable solid lasers.

In this paper, we study the photoluminescence properties of Sm^{3+}-doped nanocrysalline TiO_2 powders fabricated by the sol–gel method. Strong orange red emission of Sm^{3+} was observed due to efficient energy transfer from the TiO_2 host to Sm^{3+} ions. To tune the location of the host excitation, either Bi^{3+} or Zr^{4+} ions were codoped in the powders containing Sm^{3+} ions, which remarkably influence photoluminescence properties of TiO_2:Sm^{3+}.

*Corresponding author. Fax: +86 431 6176320.
E-mail address: hwsong2005@yahoo.com.cn (H. Song).

0022-2313/$ - see front matter © 2007 Elsevier B.V. All rights reserved.
doi:10.1016/j.jlumin.2007.01.020

2. Experiments

2.1. The synthesis of metal-ion-doped TiO_2

The TiO_2 particles were prepared with the sol–gel method, which was previously reported by Xu et al. [22]. In the preparation, tetra-*n*-butyl titanate and the RE metal salts $Sm(NO_3)_3 \cdot 5H_2O$ were chosen as the precursors. First, 12.5 ml $Ti(OBu)_4$ (C.P.) was dissolved in 33.3 ml ethanol with stirring for 10 min, then 0.25 ml HNO_3 was added dropwise to the above solution under stirring for 30 min. Another solution containing 16.7 ml ethanol, 1.5 ml H_2O, and RE metal salts in the required stoichiometry was slowly added into the above solution. The mixture was hydrolyzed at room temperature for 40 min under vigorous stirring, and the transparent sol was obtained. The gel was prepared by aging the sol for 48 h at room temperature. The derived gel was dried at 100 °C for 24 h to remove the solvents and then fired in air at 700 °C for 2 h.

Metal-ions-codoped TiO_2 sample were prepared according to the same procedure in the presence of added metal salts. Metal salts used as precursors for codoping ions are $ZrOCl_2 \cdot 8H_2O$, and $Bi(NO_3)_3 \cdot 5H_2O$. The doping concentration varied from 0.5% to 5% in molar ratio.

2.2. Characterization

X-ray diffraction (XRD) data were collected on a Rigaku D/max-rA X-ray diffractometer using a Cu target radiation source ($\lambda = 1.54078$ Å). SEM was performed on a Hitachi S4800 field-emission scanning electron microscope. Excitation and emission spectra at room temperature were measured with a Hitachi F-4500 fluorescence spectrometer. In the measurements of fluorescence dynamics, a 355-nm light pumped by the pulsed Nd:YAG laser was used as excitation source. The Nd:YAG laser was with a line width of 1.0 cm^{-1}, pulse duration of 10 ns, and repetition frequency of 10 Hz. A Spex-1403 spectrometer, a boxcar integrator, and a computer were used as recording.

3. Results and discussion

3.1. Structure and morphology of TiO_2 powders

Fig. 1 shows XRD patterns of TiO_2:Sm^{3+} powders synthesized by the sol–gel method. In the figure, all the diffraction lines are assigned to tetragonal phase of anatase. XRD patterns of TiO_2:Sm^{3+}/Bi^{3+} or TiO_2 Sm^{3+}/Zr^{4+} are similar to the TiO_2:Sm^{3+} (Sm—0.75%). No additional diffraction lines were observed, suggesting that Bi^{3+} or Zr^{4+} were doped into the TiO_2 lattices. The codoping of Bi^{3+} or Zr^{4+} has a little influence on widths of XRD patterns. Estimated by diffraction peak of (1 0 1) using Scherrer equation, the crystalline sizes for the samples TiO_2:Sm^{3+}, TiO_2:Sm^{3+}/Bi^{3+} and TiO_2 Sm^{3+}/Zr^{4+} were determined to be 27, 23 and 21 nm, respectively. The codoping of Bi^{3+} or Zr^{4+} also leads the diffraction peaks

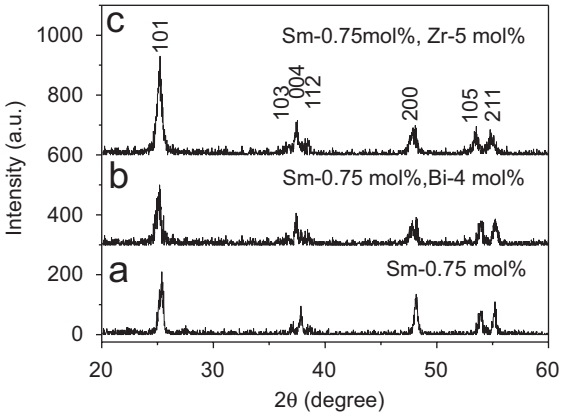

Fig. 1. XRD patterns for samples: (a) TiO_2:Sm^{3+}, (b) TiO_2:Sm^{3+}, Bi^{3+}, and (c) TiO_2:Sm^{3+}, Zr^{4+}.

to shift to the small angle direction. Owing to larger radii of Bi^{3+} ions and Zr^{4+} ions than the Ti^{4+}, the interplanar distance becomes longer in the case of codoping. Based on Bragg equation $n\lambda = 2d\sin\theta$, the diffraction angle becomes smaller.

Fig. 2 shows FE-SEM images of the three samples mentioned above. It is obvious that all the powders yield nanoparticles and they tend to aggregate together. The average grain sizes determined from the Scherrer equation are smaller than those determined from FE-SEM images. This is not strange because the size distribution in the system is inhomogeneous and smaller nanograins contribute more to the broadening of the diffraction peaks. The average particle size for the nanocrystals codoped with metal ions becomes smaller in comparison with TiO_2:Sm^{3+}. The XRD patterns and FE-SEM images both indicate that the codoped ions suppress the particle growth.

3.2. Luminescence properties of the TiO_2:Sm^{3+} nanocrytals

The excitation spectra of TiO_2:Sm^{3+} (0.75 mol%), TiO_2:Sm^{3+}/Bi^{3+}, and TiO_2:Sm^{3+}/Zr^{4+} nanocrystals monitoring the transition of $^4G_{5/2} \rightarrow {}^6H_{7/2}$ for Sm^{3+} are presented in Fig. 3a. The PL excitation spectrum of TiO_2:Sm^{3+} exhibits an intense broad band centered at 358 nm (3.4 eV), which is assigned to titania host absorption, confirming the effective energy transfer from TiO_2 host to Sm^{3+} ions. In addition, a relative weak band at 240 nm can be attributed to the charge transfer transition (CT) from the O^{2-} ligand to the Sm^{3+} ion [23]. It is well known that the band gap of bulk TiO_2 is 3.2 eV [24]. According to XRD patterns, the crystalline size of TiO_2:Sm^{3+} is about 27 nm, which is much bigger than exciton Bohr radius of TiO_2 (1.5 nm) [25]. Therefore, the effect of quantum confinement on the band gap of TiO_2 can be neglected. It is suggested that the increase in excitation energy results from the coupling of the exciton to phonon, which has been observed in other nanocrystalline systems [26]. In comparison with TiO_2:Sm^{3+} nanocrystals, the band location originated from titania

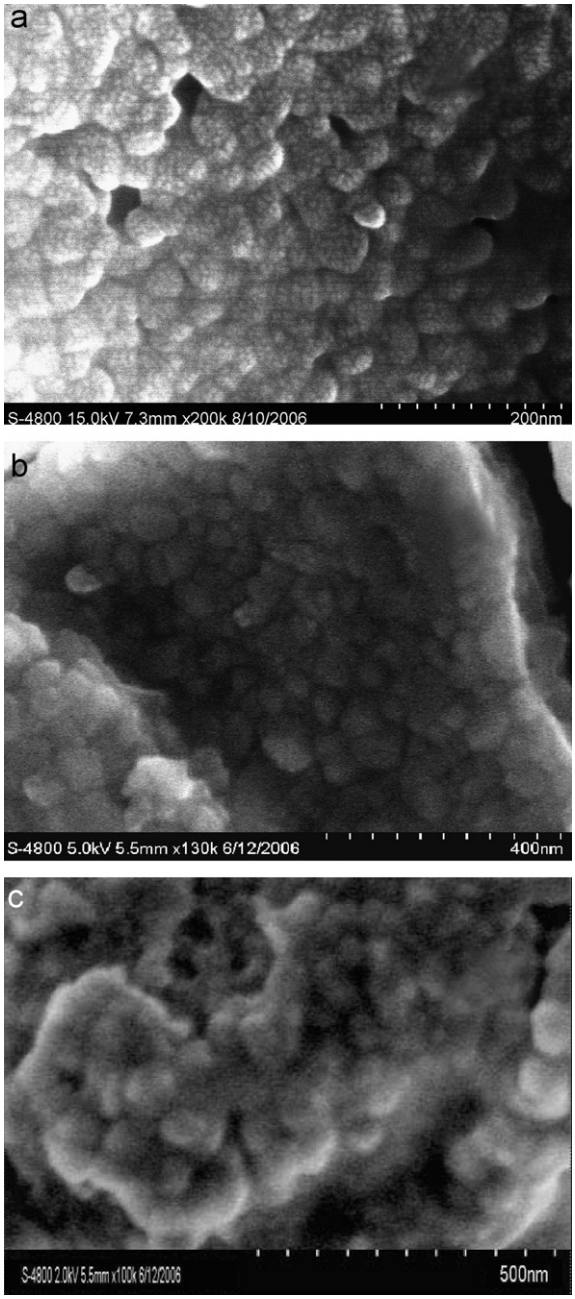

Fig. 2. SEM image of the samples: (a) TiO_2:Sm^{3+}, (b) TiO_2:Sm^{3+}/Bi^{3+}, and (c) TiO_2:Sm^{3+}/Zr^{4+}.

absorption in TiO_2:Sm^{3+}/Bi^{3+} shifts to blue, while that in TiO_2:Sm^{3+}/Zr^{4+} shifts to red. These will be discussed in the following sections.

Excitation of TiO_2:Sm^{3+} sample above the measured titania band gap results in strong characteristic emission of Sm^{3+} ions in the range of 550–720 nm, as shown in Fig. 3b. Three groups of lines centered at approximately 581, 610, and 660 nm were observed, corresponding to the transitions from the excited $^4G_{5/2}$ level to the $^6H_{5/2,7/2,9/2}$ levels, respectively. The fine structure can be explained by taking into account the ^6H_J levels that are split into $2J+1$ sublevels in the crystal field. Although the radii of RE ions seem to be too large to allow them to replace Ti^{4+} in an

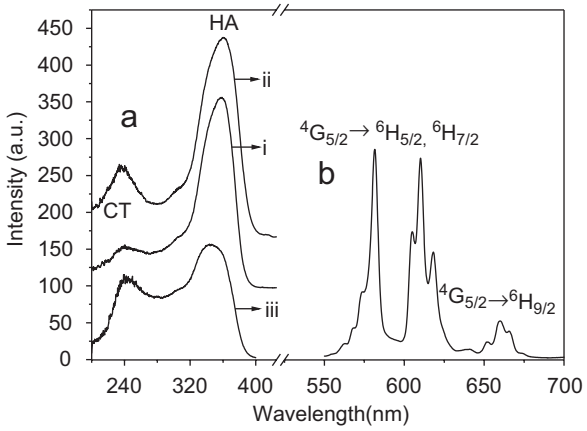

Fig. 3. (a) Excitation spectra ($\lambda_{em} = 610$ nm) for (i) TiO_2:Sm^{3+} (0.75 mol%), (ii) TiO_2:Sm^{3+} (0.75 mol%), Zr^{4+} (0.5 mol%), and (iii) TiO_2:Sm^{3+} (0.75 mol%), Bi^{3+} (0.5 mol%). (b) Emission spectrum of TiO_2:Sm^{3+} ($\lambda_{ex} = 355$ nm).

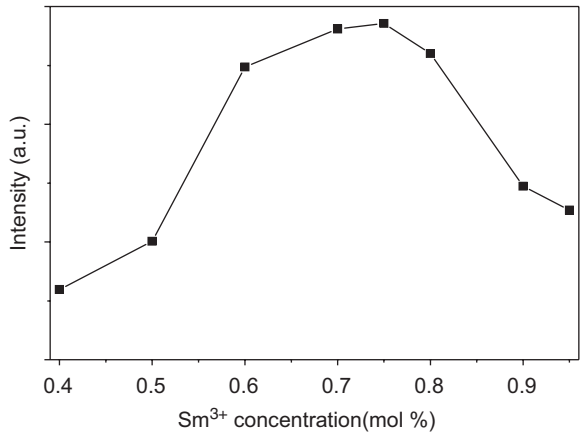

Fig. 4. Emission intensity of TiO_2:Sm^{3+} nanocrystals as a function of Sm^{3+} concentration.

anatase crystal (1.04 Å versus 0.64 Å), the well-resolved ^6H_J levels clearly demonstrate that Sm^{3+} ions are fitted into a quite regular environment, contrary to the situation encountered in amorphous matrices. It is reasonable to conclude that the Sm^{3+} ion distorts the TiO_6 octahedron substituting the Ti^{4+} ion in shifted position [12,27]. Fig. 4 shows the emission intensity for TiO_2:Sm^{3+} as a function of Sm^{3+} concentration, and the optimum Sm concentration in TiO_2 for optical emission was determined to be 0.75 mol%. The low optimum concentration is because the solubility of Sm^{3+} in the TiO_2 lattice is rather limited, which is conceivable from the quite big size discrepancy between Ti^{4+} and Sm^{3+}.

The time-resolved emission spectra of the TiO_2:Sm^{3+} sample excited under the excitation of 355 nm at room temperature were also measured, as shown in Fig. 5. Besides the emissions originated from Sm^{3+}, a broad band originating from surface defect emission of nanoscale TiO_2 powders was observed at around 490 nm, which was similar to the result reported by Zhu and Ding [28]. They prepared TiO_2 nanocrystals by similar method and observed a broad

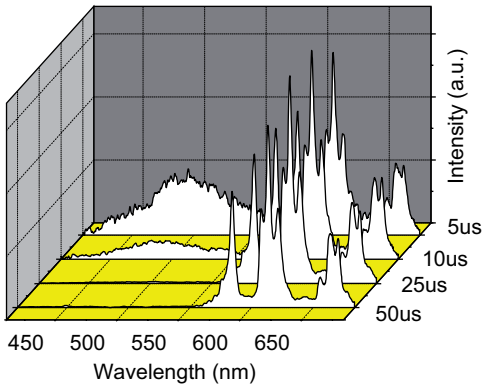

Fig. 5. Time-resolved emission spectra of the TiO_2:Sm^{3+} nanocrystals at room temperature ($\lambda_{ex} = 355$ nm).

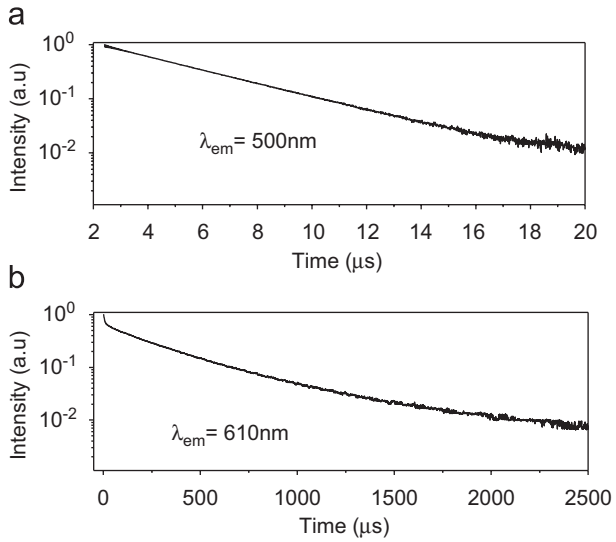

Fig. 6. Kinetic curves for (a) the TiO_2 defect emission ($\lambda_{em} = 490$ nm) and (b) $^4G_{5/2} \rightarrow {}^6H_{7/2}$ transition of Sm^{3+} ($\lambda_{em} = 610$ nm).

band emission around 475 nm and assigned it to the TiOH or $TiOC_2H_5$ surface groups. Because of lower phonon energy of the TiO_2 host and mismatch of energy levels, the excited energy of TiO_2 cannot be directly transferred to Sm^{3+} ions. Energy transfer can occur in virtue of the media defect level, which is in accordance with the model proposed by Frindell and Bartl [18]. By absorbing UV light, electrons are first excited into the conduction band of titania, to subsequently relax the TiO_2 defect states, and then to relax the crystal field states of Sm^{3+} through energy transfer.

The kinetic curves for the TiO_2 defect emission and $^4G_{5/2} \rightarrow {}^6H_{7/2}$ transition for Sm^{3+} were measured, as shown Fig. 6a and b, respectively. The decay curve for TiO_2 defect emission (about 490 nm) can be well fitted by a single-exponential function, $I = I_0 \exp(-t/\tau)$. Here, τ is determined to be 3.4 μs. The decay curve for main emission $^4G_{5/2} \rightarrow {}^6H_{7/2}$ (610 nm) of Sm^{3+} (Fig. 7b) can be well fitted by a bi-exponential function, $I = I_1 \exp(-t/\tau_1) + I_2 \exp(-t/\tau_2)$. The two decay time constants were determined to be $\tau_1 = 11.4$ μs and $\tau_2 = 346.2$ μs. The non-exponential decay

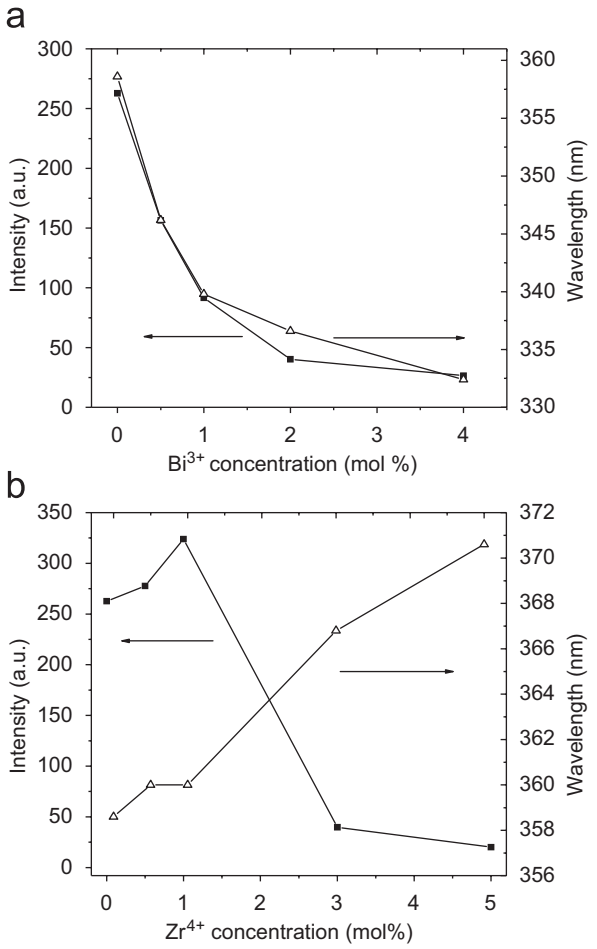

Fig. 7. Dependence of intensity and wavelength of central excitation band on (a) Bi^{3+} and (b) Zr^{4+} ions concentration.

behavior of the activator is frequently observed when energy transfer occurs or when the photoluminescence is contributed by different origins. Presently, the band originated from defect states may also contribute to the emission at 610 nm, which owns a decay time constant of several microseconds.

3.3. Luminescence properties of TiO_2:Sm^{3+}, Bi^{3+}, and TiO_2:Sm^{3+}, Zr^{4+} samples

The codoping of Bi^{3+} or Zr^{4+} has influence not only on the location of excitation band, but also on the fluorescence intensity and dynamics. Fig. 7a and b shows, intensity and central location of excitation band as a function of Bi^{3+} or Zr^{4+} ions concentration, respectively, in TiO_2:Sm^{3+}/Bi^{3+} or TiO_2:Sm^{3+}/Zr^{4+}. It can be seen from Fig. 7(a) that, as the Bi^{3+} concentration increases, the excitation band of TiO_2 shifts to blue gradually. Especially for TiO_2:Sm^{3+} (Sm—0.75 mol%) codoped with 4 mol% Bi^{3+}, the central excitation wavelength for the TiO_2 host absorption shifts to 332.4 nm from the location of 358 nm in the case without Bi^{3+} codoping. Blue shift (26 nm) was observed. This phenomenon is attributed to an increase in exciton–phonon coupling resulting from the suppression effect of codoped

Bi^{3+} ions on particle size [26]. With the increase in Zr^{4+} concentration, a red shift of the central excitation wavelength of the host absorption occurs (Fig. 7b). When the concentration of codoped Zr^{4+} ions reaches 5 mol%, the central excitation band is remarkably tuned to 370 nm (Fig. 7b), which matches GaN ultraviolet diode laser. Presumably, these red shifts resulted from defects caused by trace amounts of Zr^{4+} in the TiO_2 lattice [29]. It should be noted that in the codoped systems of Zr^{4+} or Bi^{3+} ions, the photoluminescence of Sm^{3+} was quenched.

To study the decay behaviors of Sm^{3+} luminescence in the TiO_2:Sm^{3+}, Bi^{3+}, and TiO_2:Sm^{3+}, Zr^{4+} phosphors, the kinetic curves for the Sm^{3+} representative emission of $^4G_{5/2} \rightarrow {}^6H_{7/2}$ (610 nm) were measured. The decay curves for both phosphors can be fitted into the bi-exponential function. The lifetime constant versus Bi^{3+} concentration in the TiO_2:Sm^{3+}, Bi^{3+} nanocrystals is drawn in Fig. 8. It can be seen that the lifetime initially increases with increasing concentration, and it then approaches a maximum at the concentration of 1 mol% (Bi concentration), and then it decreases as the doping concentration increases further. The case for the fluorescence dynamics of TiO_2:Sm^{3+}, Zr^{4+} phosphor is similar.

It is easier to understand that the fluorescence lifetime decreases with the increase in Bi^{3+} or Zr^{4+} concentration. On the one hand, the Bi^{3+} or Zr^{4+} ions may act as fluorescence killers due to the energy transfer from excited Sm^{3+} to Bi^{3+} or Zr^{4+} ions. On the other hand, the codoping leads the average particle size of TiO_2 to decrease. More surface defects will be involved and the non-radiative relaxation rate will increase. Presently, the increase in fluorescence lifetime with codoping concentration (as the codoping concentration is smaller) has not been fully understood. A small part of codoping will not only induce the crystal field, but also cause the defect states to change, which largely influences the transition processes. Hence, it remains as an open question.

Based on the model given by Frindell and Bartl [18], a modified model (Fig. 9) for the energy transfer in this codoping system was proposed. The codoping of metal ions

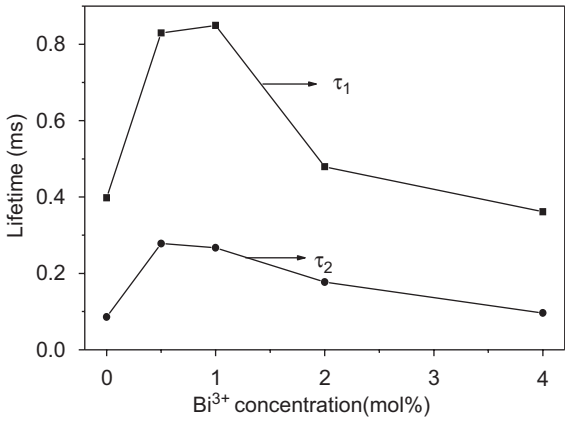

Fig. 8. Dependence of fluorescence lifetime of the $^4G_{5/2}$ state in TiO_2:Sm^{3+}, Bi^{3+} nanocrystals on Bi^{3+} concentration.

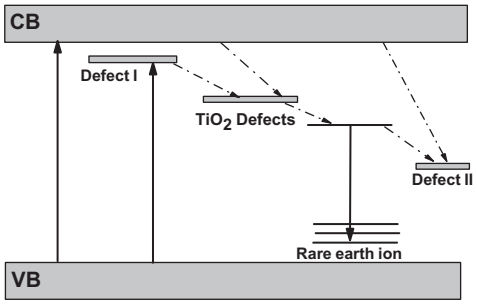

Fig. 9. Proposed mechanism for energy transfer and photoluminescence in codoped TiO_2 nanocrystals.

(Bi^{3+} ions or Zr^{4+} ions) makes the Sm^{3+} luminescence quench and the lifetime (Sm $^4G_{5/2} \rightarrow {}^6H_{7/2}$) decrease. The central excitation wavelength of the host shifts to red when codoping with Zr^{4+} ions. According to these experimental phenomena, we suggest that two kinds of defects were introduced by codoping. One class of defect (defect I) locates near the conduction region (induced by codoping of Zr^{4+}). Electrons are excited to the level of defect I that results in the red shift of excitation band. Another class of defect (defect II), induced by Bi^{3+} or Zr^{4+} codoping, is situated below the excitation state of Sm^{3+} ions. Fluorescence quenching caused by codoping can be interpreted by non-radiative relaxation of electrons in the conduction band to defect II, as well as the energy transfer from excited states of Sm^{3+} to the defect II, which can be revealed by the fluorescence dynamics.

Note that the photoluminescence properties of TiO_2:Sm^{3+} codoped with other metal ions, such as Zn^{2+}, Cr^{3+} etc., were also studied. Similar to Bi^{3+} or Zr^{4+} codoped ones, the excitation wavelength was also tuned by codoping; however, the emission intensity of Sm^{3+} was quenched due to codoping.

4. Conclusions

Samarium and metal ions-doped TiO_2 semiconductor was synthesized by the sol–gel method. Effective energy transfer from TiO_2 to Sm^{3+} was observed. The optimum Sm^{3+} concentration in TiO_2 for optical emission was determined to be 0.75 mol%. The photoluminescence and energy transfer mechanism were discussed. It was observed that the central wavelength of TiO_2 hosts absorption in TiO_2:Sm^{3+}/Bi^{4+} shifted to the shorter wavelength with the increase in Bi^{3+} concentration, while it shifted to red in the TiO_2:Sm^{3+}/Zr^{4+}. It is believed that codoped TiO_2:Sm^{3+} can be a candidate for white LED and tunable solid lasers. Further work should be performed to increase the photoluminescence intensity of the nanocrystalline system.

Acknowledgements

This work is supported by the National Nature Science Foundation of China (Grants 10374086 and 10504030) and Talent Youth Foundation of JiLin Province (Grants 20040105).

References

[1] M.J. Denjeka, B. Samson, Mater. Res. Soc. Bull. 8 (1999) 39.
[2] W.M. Jadwisienczak, H.J. Lozykowski, Appl. Phys. Lett. 76 (2000) 3376.
[3] F. Lu, R. Carius, A. Alam, J. Appl. Phys. 92 (2002) 2457.
[4] E.E. Nyein, U. Hommerich, Appl. Phys. Lett. 82 (2003) 1655.
[5] S. Komuro, T. Katsumata, Appl. Phys. Lett. 76 (2000) 3935.
[6] E. De la Rosa-Cruz, L.A. Diaz-Torres, J. Appl. Phys. 94 (2003) 3509.
[7] S. Jeon, P.V. Braun, Chem. Mater. 15 (2003) 1256.
[8] J.W. Stouwdam, F.C.J.M. van Veggel, Chem. Phys. Chem. 5 (2004) 743.
[9] M.A. Fox, M.T. Dulay, Chem. Rev. 93 (1993) 341.
[10] C. Urlacher, J. Mugnier, J. Raman Spectrosc. 27 (1996) 785.
[11] V. Kiisk, I. Sildos, S. Lange, Appl. Surf. Sci. 247 (2005) 412.
[12] S. Lange, I. Sildos, V. Kiisk, Mater. Sci. Eng. B 112 (2004) 87.
[13] V. Reedo, S. Lange, V. Kiisk, Proc. SPIE 5946 (2006) 59460F-1.
[14] C.C. Ting, S.Y. Chen, J. Appl. Phys. 90 (2001) 5564.
[15] R. Palomino-Merino, A. Conde-Gallardo, Thin Solid Films 401 (2001) 118.
[16] J. Ovenstone, P.J. Titler, R. Withnall, J. Phys. Chem. B 105 (2001) 7170.
[17] C.W. Jia, E.Q. Xie, J.G. Zhao, J. Appl. Phys. 100 (2005) 023529.
[18] K.L. Frindell, M.H. Bartl, J. Solid State Chem. 172 (2003) 81.
[19] K.L. Frindell, M.H. Bartl, A. Popitsch, Angew. Chem. Int. Ed. 41 (2002) 959.
[20] A. Conde-Gallardoa, M. García-Rocha, Appl. Surf. Sci. 212 (2003) 583.
[21] C.-y. Wang, D.W. Bahnemann, Chem. Commun. 16 (2000) 1539.
[22] A.-W. Xu, Y. Gao, H.-Q. Liu, J. Catal. 207 (2002) 151.
[23] B. Lei, Y. Liu, G. Tang, Mater. Chem. Phys. 87 (2004) 227.
[24] A.G. Agrios, K.A. Gray, Langmuir 19 (2003) 1402.
[25] D. Pan, N. Zhao, Q. Wang, Adv. Mater. 17 (2005) 1991.
[26] A. Konrad, U. Herr, R. Tidecks, J. Appl. Phys. 90 (2001) 3516.
[27] S. Makishima, H. Yamamoto, T. Tomotsu, J. Phys. Soc. Jpn. 20 (1965) 2147.
[28] Y.C. Zhu, C.X. Ding, J. Solid State Chem. 145 (1999) 711.
[29] S.M. Chang, R.A. Doong, J. Phys. Chem. B 110 (2006) 20808.